Lipid nanoparticles with ionizable lipids: Statistical aspects

Downloaded from: https://research.chalmers.se, 2026-10-08 20:03 UTC

Citation for the original published paper (version of record):
Zhdanov, V. (2022). Lipid nanoparticles with ionizable lipids: Statistical aspects. Physical Review E, 105(4). http://dx.doi.org/10.1103/PhysRevE.105.044405

N.B. When citing this work, cite the original published paper.

research.chalmers.se offers the possibility of retrieving research publications produced at Chalmers University of Technology. It covers all kind of research output: articles, dissertations, conference papers, reports etc. since 2004. research.chalmers.se is administrated and maintained by Chalmers Library

(article starts on next page)

Lipid nanoparticles with ionizable lipids: Statistical aspects

Vladimir P. Zhdanov *

Section of Nano and Biophysics, Department of Physics, Chalmers University of Technology, Göteborg, Sweden and Boreskov Institute of Catalysis, Russian Academy of Sciences, Novosibirsk, Russia

(Received 23 January 2022; accepted 4 April 2022; published 20 April 2022)

Lipid nanoparticles (LNPs) with size ∼100 nm are now used for fabrication of a new generation of drugs and antiviral vaccines. To optimize their function or, more specifically, interaction with cell membranes, their composition often includes ionizable lipids which are neutral or cationic (after association with H^+). Physically, such LNPs represent an interesting example of mesoscopic nanosystems with complex and far from understood properties. Experimentally, they can be studied at cell-membrane mimics. Herein, I analyze theoretically three related aspects. (i) I describe how the extent of protonation of ionizable lipids located at the surface of LNPs depends on the H^+ concentration by using the phenomenological Langmuir-Stern and Poisson-Boltzmann models with continuum distribution of charges and the dipole model with discrete charges. In these frameworks, the H^+ adsorption isotherms are predicted to be close to Langmuirian provided the fraction of ionizable lipids is smaller than 0.5. (ii) I scrutinize the interaction between charged LNPs and their interaction with a supported lipid bilayer (SLB) by using the phenomenological theory and lattice-gas model. The long-term association or attachment is predicted provided the charges are opposite. The models make it possible to estimate the size of the contact region (provided a LNP is not deformed) and the number of lipid-lipid bonds in this region. (iii) I briefly discuss denaturation of a LNP during interaction with the SLB and argue that it may occur via a few stepwise transitions.

DOI: 10.1103/PhysRevE.105.044405

I. INTRODUCTION

Nanoscience is now flourishing. In particular, there are numerous efforts to use nanoparticles in various biomedical applications (reviewed in [1–3]). In this area, 100-nm-sized lipid nanoparticles (LNPs) have attracted appreciable attention in the context of fabrication of novel drugs and antiviral vaccines based on RNA (mRNA or siRNA) delivery [4]. *In vivo*, after penetration the outer cell membrane, LNPs are often trapped and processed at anionic membranes of endosomes in a not fully understood manner [5,6]. One of the practical problems here is that only a small amount of LNPs appear to be able to escape from endosomes and to release the content, and accordingly the endosomal escape is crucial for efficient RNA delivery and function [4]. Experiments with advanced cellular assays have allowed one to formulate conceptual mechanisms of the endosomal escape (reviewed in [7–9]). The proposed pathways include membrane fusion, osmotic pressure effects, particle swelling, and membrane destabilization [7]. The mechanistic details of such processes can be studied at cell-membrane mimics such as a supported lipid bilayer (SLB) [10].

To influence and/or regulate the endosomal escape, LNPs can be composed with participation of ionizable lipids which are neutral at physiological *p*H and protonated, i.e., positively charged, at lower *p*H [4]. The former reduces the interaction with the anionic membranes of cells. The latter facilitates electrostatic interaction and fusion of LNPs with negatively charged endosomal membranes, resulting in the leak of mRNA molecules into the cytoplasm. Conceptually, the leak can be interpreted in terms of the fusion-pore or transient-pore models [8]. The specifics of such systems are of interest from the perspectives of physics in general and statistical physics in particular.

Some aspects of the function of LNPs have already been clarified by using the corresponding biophysical models (see, e.g., Refs. [11–21]). The models of this category focused on LNPs containing ionizable lipids are, however, lacking. Herein, I fill this gap to some extent. In particular, I first describe how the extent of protonation of ionizable lipids located at the surface of LNPs depends on the H^+ concentration (Sec. II) and then discuss the interaction between positively and negatively charged LNPs and their interaction with an SLB (Sec. III). In addition, I briefly discuss the likely scenarios of denaturation of LNPs during their interaction with a lipid bilayer (Sec. IV). These aspects are of interest in the context of academic studies of LNPs at cell-membrane mimics and some of them are relevant in the context of applications as well. From the perspective of statistical physics, the problems under consideration are complex and can be

*zhdanov@chalmers.se

Published by the American Physical Society under the terms of the Creative Commons Attribution 4.0 International license. Further distribution of this work must maintain attribution to the author(s) and the published article's title, journal citation, and DOI. Funded by Bibsam.

tackled at different levels by using various approximations. In Secs. II and III, I first use phenomenological models with continuum (averaged) distribution of charges and then more specific models with interaction between discrete charges located at lipids. The LNP denaturation (Sec. IV) is discussed at the phenomenological coarse-grained level.

II. EXTENT OF PROTONATION OF IONIZABLE LIPIDS

A. General remarks

LNPs containing RNA are spherically shaped aggregates. At the coarse-grained level, depending on composition, their structure may be different. The exterior part of a LNP is often viewed as a lipid bilayer. The poorly ordered internal part can (i) be reminiscent of multilamellar vesicles with solution and RNA located between lipid leaflets [22], (ii) exhibit more complex and less ordered domains of "cubic" phase, formed by a lipid bilayer and containing water channels [23], or (iii) exhibit "inverse hexagonal" phase [24]. Accurate description of ionizable lipids in such structures is challenging. Suitable models can be formulated but the corresponding full-scale analysis can be done only numerically even in the simplest case of combination of spherical shells representing lipid leaflets and the regions between them. As the first step in this direction, I analyze the extent of protonation of ionizable lipids at the external surface of LNPs.

After protonation, the ionizable lipids become positively charged. For global electroneutrality, the positive charges of lipid heads are compensated by negative charges belonging to the solution. Physically, it can be done in a different way. One limit is when the positive charges of lipids are balanced by negative charges continuously distributed in solution. This limit can be described by using combination of the Langmuir-Stern model for H^+-lipid-head association with the Poisson-Boltzmann model for charge distribution in solution. Another limit is when the positive charge of each lipid head is balanced locally by a negative charge with well defined relative location, so that these charges form a dipole. The latter limit can be described by employing the dipole approximation. Focusing on the external surface of LNPs, I analyze both these limits in Secs. II B and II C, respectively, because now there are no clear indications in favor of one of them. In both cases, the charges located inside a LNP, i.e., on the internal lipid layers and solution between them, are ignored. The role of the latter charges is briefly discussed later on in Sec. II D.

B. Langmuir-Stern and Poisson-Boltzmann models

The Langmuir-Stern model is one of the seminal models in electrochemistry (reviewed in [25]). It is not, however, widely used in general and was not used to describe LNPs with ionizable lipids in particular. In this model, the probability that a lipid is ionized, i.e., that its head contains H^+, is given by

$$p = c_{H^+}/[K_a \exp(e\varphi/k_BT) + c_{H^+}], \tag{1}$$

where c_{H^+} is the H^+ concentration in solution, e is the absolute value of the electron charge, φ is the potential at the lipid head, and K_a° is the H^+ attachment-detachment constant at $\varphi = 0$. This expression for p does not specify how the potential is calculated and accordingly can be used in various situations. In the context under consideration, it can be employed to describe the external surface of a LNP. At this interface, the surface concentration of the positive charge is given by

$$q = \frac{e\chi p}{s} \equiv \frac{e\chi c_{H^+}}{s\{K_a \exp[e\varphi/k_BT] + c_{H^+}\}}, \tag{2}$$

where χ is the fraction of the ionizable lipids and $s = 0.6\ \mathrm{nm}^2$ is the surface area per lipid.

The electric field generated by the ionizable lipid near the LNP-solution interface is $4\pi q/\epsilon_s$, where $\epsilon_s = 80$ is the solution permittivity. The potential φ introduced above can be identified with that at this interface. The double layer near the interface can, on the other hand, be described by using the Poisson-Boltzmann model. Under physiological conditions, the radius of a LNP (∼50 nm) is much larger than the Debye length [$\delta = (\epsilon_s k_BT/8\pi e^2 c_\circ)^{1/2} \sim 1$ nm], and accordingly the interface can be considered to be flat. In this case, the electric field at the interface is given by the the Grahame equation (Section 13.3.2 in [26]),

$$\frac{4\pi q}{\epsilon_s} = \left(\frac{32\pi k_BT c_\circ}{\epsilon_s}\right)^{1/2} \sinh\left(\frac{e\varphi}{2k_BT}\right), \tag{3}$$

where $c_\circ$ is the concentration of positive or negative charges in solution (1:1 electrolyte).

Substituting (3) into (2) yields

$$\frac{\chi c_{H^+}}{K_a \exp[e\varphi/k_BT] + c_{H^+}} = \left(\frac{2\epsilon_s k_BT s^2 c_\circ}{\pi e^2}\right)^{1/2} \sinh\left(\frac{e\varphi}{2k_BT}\right). \tag{4}$$

This equation allows one to calculate φ as a function of other parameters. The probability that a lipid is ionized can then be calculated by using Eq. (2). The results of such calculations are shown in Fig. 1 for the physiological value of the electrolyte concentration, $c_\circ = 150$ mM, and $\chi = 0$, 0.1, 0.3, and 0.5. If $\chi = 0$, the double layer is negligible, i.e., $\varphi = 0$, and Eq. (2) is reduced to the Langmuir adsorption isotherm. With increasing χ, the isotherm becomes non-Langmuirian. If χ is appreciable, e.g., 0.5, the deviation from the Langmuir isotherm is well manifested.

C. Dipole model

The Langmuir-Stern and Poisson-Boltzmann models used above are phenomenological. The conditions of their applicability can be and were debated from various perspectives (see e.g. [25,27–30]). One of the shortcomings of the Poisson-Boltzmann model is that it does not take spatial constraints on the arrangement of ions and can overestimate the local ion concentration near the interfaces [27]. From this perspective, the Poisson-Boltzmann model can be extended by using various approximations [27,29]. This shortcoming is important in the case of strong electrolytes (large surface potentials) and/or asymmetric ion charges and sizes. In biologically relevant situations, electrolytes can usually be classified as weak, and accordingly the role of spatial constraints is not central. What can be more important is that the Poisson-Boltzmann model implies that the surface charge as well as the charges in solution near an interface are distributed continuously. In the case of LNPs, the surface charge are, however, located

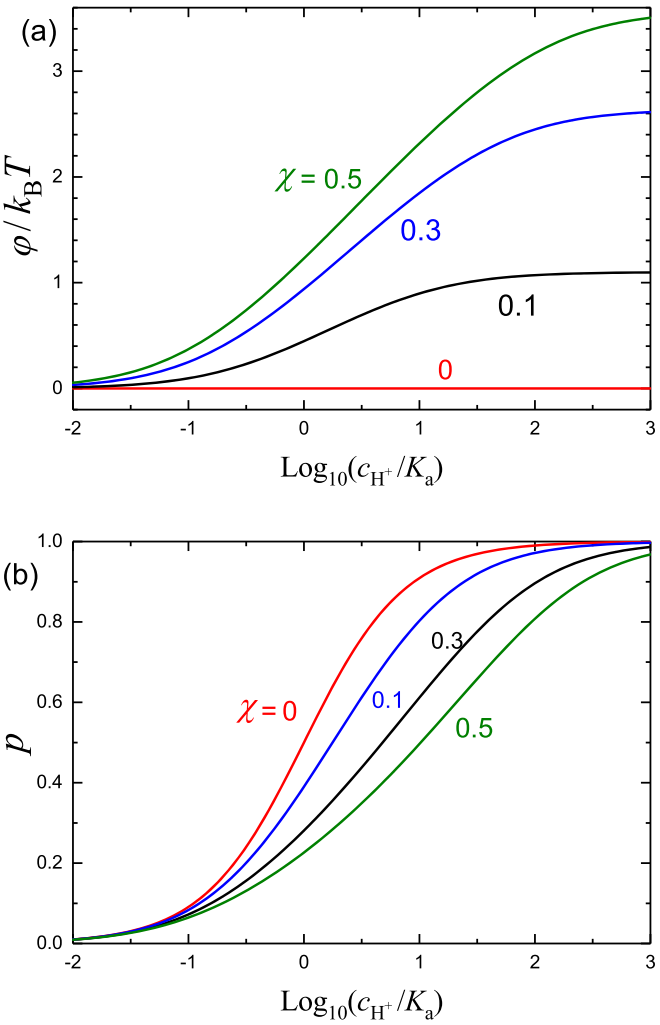

FIG. 1. (a) Normalized potential and (b) probability that an ionizable lipid is in the cationic state as a function of the normalized H^+ concentration according to the Langmuir-Stern and Poisson-Boltzmann models with $T = 300$ K, $c_\circ = 150$ mM, and $\chi = 0$, 0.1, 0.3, and 0.5.

at lipids and, strictly speaking, should be described by using the corresponding models with interaction between discrete charges located at lipids. It can be done at different levels (see, e.g., [30]). To keep the analysis and results compact, I employ one of the versions of the dipole approximation as it was earlier used in the context in surface science [31].

In the framework of the dipole approximation, Eq. (1) is replaced by

$$p = c_{H^+}/[K_a \exp(E_{dd}/k_BT) + c_{H^+}], \tag{5}$$

where E_{dd} is the energy of the repulsive (positive) interaction of a dipole with other dipoles. In the case of firm dipoles at a flat interface, this energy is given by (see Eq. (11) in [31])

$$E_{dd} = \frac{\eta d^2 N^{3/2}}{\epsilon_s} \equiv \frac{\eta d^2 \chi^{3/2} p^{3/2}}{\epsilon_s s^{3/2}}, \tag{6}$$

where $N \equiv \chi p/s$ is the surface concentration of ionizable lipids in the cationic state, $d = el$ is the dipole moment (l is the corresponding length), and $\eta = 22$ is the dimensionless

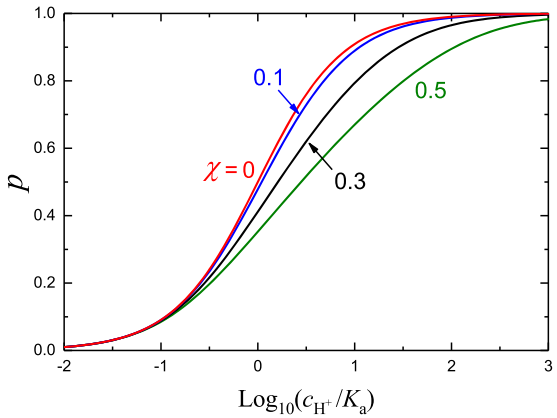

FIG. 2. Probability that an ionizable lipid is in the cationic state as a function of the normalized H^+ concentration according to the dipole model with $T = 300$ K, $l = 0.5$ nM, and $\chi = 0$, 0.1, 0.3, and 0.5.

numerical coefficient obtained after summation. Substituting (6) into (5) results in

$$p = c_{H^+} \Big/ \left[K_a^\circ \exp\left(\frac{\eta d^2 \chi^{3/2} p^{3/2}}{\epsilon_s s^{3/2} k_B T} \right) + c_{H^+} \right]. \tag{7}$$

The isotherms predicted by this equation with physically reasonable parameters are qualitatively similar to those given by Eq. (2) [cf. Figs. 2 and 1(b)]. Quantitatively, however, the deviation from the Langmuir adsorption observed with increasing χ is now slightly weaker.

D. Charges inside a LNP

In the analysis above, the focus is on the external surface of a LNP. The charges located inside a LNP are ignored. In reality, the latter charges may or may not be important depending on H^+ concentration, other parameters, and the type of arrangement of lipids inside LNPs. For example, these charges can be ignored provided their location is spherically symmetric and a LNP is globally neutral inside. In this case, according to the Gauss theorem, the charges located inside a LNP do not create an electric field at the external surface of a LNP and accordingly do not influence the extent of protonation of the ionizable lipids at the latter interface.

The role of the charges located inside a LNP is expected to increase with increasing H^+ concentration. At very high H^+ concentration, an appreciable part of ionizable lipids located both at the external interface and inside is expected to be protonated, and LNPs are expected to be unstable. From the perspective of applications of LNPs, this limit is not of interest, and attention should be focused instead on intermediate H^+ concentrations corresponding to partial protonation of ionizable lipids at the external interface. Under such conditions, the driving force for protonation is modest, and the role of protonation of ionizable lipids located inside may be minor because the heads of these lipids are separated from the heads of the lipids located at the external LNP surface by a dielectric region with relatively low permittivity (compared to that of solution), and accordingly the effect of the permittivity on the electric field is there increased, the increment of the potential

is increased as well, and the concentration of protonated lipids is reduced as predicted, e.g., by Eq. (1).

To scrutinize the role of the charges located inside a LNP, one can generalize the models described in Secs. II B and II C. Although it can easily be done, the corresponding equations are cumbersome and their numerical solution is more or less straightforward only in the spherically symmetrical case. Physically, this means that that a LNP should be viewed as a multilamellar vesicle and represented as a sphere formed of shells mimicking lipid leaflets with solution between them. Then, one can combine the Langmuir-Stern and Poisson-Boltzmann models (as in Sec. II B). The corresponding analysis confirms the qualitative conclusions drawn above [32].

III. LNP-LNP AND LNP-SLB INTERACTION

In the context of applications of positively and negatively charged LNPs, it is instructive to know the specifics and scale of interaction between them. The interaction with a charged SLB is of interest as well from the perspective of academic studies. Below, I present some estimations of these interactions by using the conventional continuum DLVO-type theory (Sec. III A) and the complementary lattice-gas model (Sec. III B).

A. DLVO-type interaction

In the DLVO-type theory [33], named after Derjaguin, Landau, Verwey, and Overbeek, the interaction between nanoparticles or between a nanoparticle and the substrate is represented as a sum of the double-layer (dl), hydration (h), and van der Waals (vdW) parts,

$$U = U_{\rm dl} + U_{\rm h} + U_{\rm vdW}, \tag{8}$$

and one can employ the Derjaguin approximation for calculation of $U_{\rm dl}$ and $U_{\rm h}$ and the Hamaker approximation for $U_{\rm vdW}$. LNPs can be considered to be spherical, and the corresponding counterparts of the interaction between them are given by [33]

$$U_{\rm dl} = \frac{r_1 r_2 \epsilon_s \varphi_1 \varphi_2}{r_1 + r_2} \exp(-d/\delta), \tag{9}$$

$$U_{\rm h} = \frac{2\pi r_1 r_2 A}{\alpha(r_1 + r_2)} \exp(-\alpha d), \tag{10}$$

$$U_{\rm vdW} = -B\phi(r_1, r_2, d)/6, \quad \text{with} \tag{11}$$

$$\phi(r_1, r_2, d) \equiv \frac{2r_1 r_2}{2(r_1 + r_2)d + d^2} + \frac{2r_1 r_2}{4r_1 r_2 + 2(r_1 + r_2)d + d^2} + \ln\left[\frac{2(r_1 + r_2)d + d^2}{4r_1 r_2 + 2(r_1 + r_2)d + d^2}\right], \tag{12}$$

where r_1 and r_2 are the LNP radii, d is the minimal LNP-LNP distance, φ_1 and φ_2 are the potentials at the LNP surfaces, α and A are the parameters determined via the energy of the hydration interaction (per unit area) of the flat interfaces [$U_h = A\exp(-\alpha d)$], and B is the lipid-lipid Hamaker constant. Physically reasonable values of some of these parameters are $\delta = 0.8$ nm (for $c_\circ = 150$ mM); $A = 0.03\,{\rm J/m^2}$ and $\alpha = 3.8\,{\rm nm^{-1}}$ [34]; and $B = 0.5 \times 10^{-20}$ J (or $\simeq 1.3 k_{\rm B}T$) [35]. The interaction between oppositely charged 80-nm-sized LNPs ($r_1 = r_2 = 40$ nm) calculated by using the equations above with these parameters and relatively weak potentials, $\varphi_1 = -\varphi_2 = k_{\rm B}T/e$, is rather weak, $\sim 7 k_{\rm B}T$ [Fig. 3(a)]. With increasing the potentials, e.g., up to $\varphi_1 = -\varphi_2 = 2k_{\rm B}T/e$, it will be about four times larger.

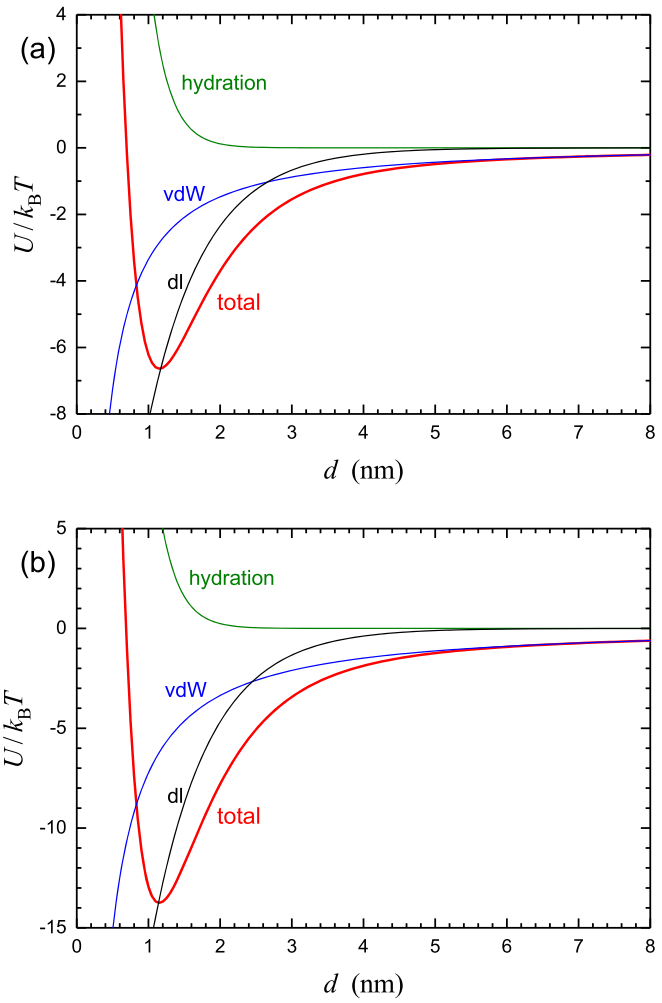

FIG. 3. (a) DLVO-type interaction between oppositely charged 80-nm-sized LNPs as a function of the minimal distance between them. The double-layer, hydration, and van der Waals interactions are shown by thin solid lines. The whole interaction is represented by a thick solid line. (b) As (a) for the the interaction between a positively charged 80-nm-sized LNP and a negatively charged SLB. The parameters are given in the text.

In academic studies, an SLB is often fabricated on a SiO_2 support. In this context, it is of interest that the SiO_2-SiO_2 Hamaker constant, $B = 0.2 \times 10^{-20}$ J [34], is comparable to that corresponding to lipid (the value of the latter has already been mentioned above). The lipid-SiO_2 Hamaker constant is approximately equal to one half of the sum of these constants and accordingly is close to the lipid-lipid Hamaker constant. Under this condition, one can use the lipid-lipid Hamaker constant for the lipid-SiO_2 Hamaker constant in order to simplify calculations. The interaction of a LNP with the SLB can then be described by employing Eqs. (8)–(12) and associating subscripts 1 and 2 with lipid and SiO_2, r_1 with the given LNP radius, and $r_2 = \infty$ with the radius corresponding to

the SLB. With this specification, the interaction between an 80-nm-sized LNP and the SLB with $\varphi_1 = -\varphi_2 = k_B T/e$ is modest, $\sim 14 k_B T$ [Fig. 3(b)]. This value is two times larger than that in the LNP-LNP case [Fig. 3(a)]. With increasing the absolute values of φ_1 and/or φ_2, these interactions will be larger.

In the case of oppositely charged LNPs or a LNP and SLB, the potential defined by Eqs. (8)–(12) can be used to describe the LNP detachment events. In particular, the maximum absolute value of this potential, $|U_*|$, can be identified with the detachment activation energy, E_a, and the corresponding rate constant can be represented as

$$k_d = \nu \exp(-E_a/k_B T) = \nu \exp(-|U_*|/k_B T), \tag{13}$$

where ν is the properly defined preexponential factor. For the LNPs under consideration, $|U_*|$ is determined primarily by the double-layer and hydration interactions. Both these interactions are proportional to $r_1 r_2/(r_1 + r_2)$. Thus, the detachment activation energy is proportional to $r_1 r_2/(r_1 + r_2)$ as well, i.e., it can be represented as

$$E_a = \frac{r_1 r_2}{r_1 + r_2} F, \tag{14}$$

where F is a function dependent on other parameters.

In the DLVO-type treatment, the attraction between oppositely charged LNPs of the size under consideration or between a LNP and SLB is related primarily to the double-layer term or, more specifically, to φ_1 and φ_2. These potentials are considered as parameters. In applications of the theory, these potentials are often identified with those corresponding to separate LNPs or a LNP and SLB. In reality, the interaction between LNPs or a LNP and SLB can be accompanied by redistribution of ionizable or charged lipids (along the interfaces) and change of the extent of ionization of the former lipids. The full-scale analysis of these effects is far from simple. Some analytical results can be obtained by using the lattice-gas model as described below.

B. Lattice-gas model

The LNPs under consideration are relatively large, and the curvature of the lipid bilayer located at their surface is low. The SLB is flat. In both cases, neutral and ionizable or charged lipids forming the external leaflet can be viewed as a two-component fully packed 2D lattice gas.

Let us first consider a separate LNP or SLB containing neutral and charged (anionic) lipids. The external SLB leaflet containing these lipid can be considered to be fully packed, and each site of the corresponding lattice is occupied by one neutral or charged lipid. The neutral lipids can be viewed as a background for charged lipids. Thus, the latter lipids can be described as a conventional lattice gas with the effective chemical potential, μ_{al}. In the mean-field approximation, it can be done at the level of a single site. In particular, the corresponding one-site grand canonical function is represented as as a sum of two terms corresponding, respectively, to the background and an anionic lipid,

$$S_{al} = 1 + \exp\left(\frac{\mu_{al} - E_{al}}{k_B T}\right), \tag{15}$$

where $E_{al} < 0$ is the interaction of an anionic lipid with other anionic lipids and charges in solution. According to the grand canonical distribution, the fraction of anionic lipids, θ_{al}, is expressed via the chemical potential as

$$\theta_{al} = \exp\left(\frac{\mu_{al} - E_{al}}{k_B T}\right) \Big/ S_{al}. \tag{16}$$

In combination with Eq. (15), this expression can be rewritten in terms of the dependence of the chemical potential on θ_{al},

$$\exp\left(\frac{\mu_{al} - E_{al}}{k_B T}\right) = \frac{\theta_{al}}{1 - \theta_{al}}. \tag{17}$$

Second, let us consider a separate LNP containing neutral and ionizable lipids. The neutral lipids can again be viewed as a background. The ionizable lipids can be characterized by the effective chemical potential, μ_{il}. In this case, the one-site grand canonical function is represented as as a sum of three terms corresponding, respectively, to the background, an ionizable lipid in the neutral state, and the latter lipid in the cationic state (in association with H^+),

$$S_{il} = 1 + \exp\left(\frac{\mu_{il}}{k_B T}\right) + \exp\left(\frac{\mu_{il} + \mu_{H^+} - E_{il}}{k_B T}\right), \tag{18}$$

where $E_{il} < 0$ is the interaction of an ionized lipid with other ionized lipids and charges in solution, and

$$\mu_{H^+} = k_B T \ln(c_{H^+}) + \varsigma \tag{19}$$

is the H^+ chemical potential (ς is the corresponding properly defined constant). The fraction of ionizable lipids, θ_{il}, is accordingly given by

$$\theta_{al} = \exp\left(\frac{\mu_{il}}{k_B T}\right)\left[1 + \exp\left(\frac{\mu_{H^+} - E_{il}}{k_B T}\right)\right] \Big/ S_{il}. \tag{20}$$

In combination with Eq. (18), this expression can be rewritten as

$$\exp\left(\frac{\mu_{il}}{k_B T}\right)\left[1 + \exp\left(\frac{\mu_{H^+} - E_{il}}{k_B T}\right)\right] = \frac{\theta_{il}}{1 - \theta_{il}}. \tag{21}$$

Let us now consider the situation when a spherically shaped LNP containing ionizable lipids contacts a spherically shaped lipid (with radii r_1 and r_2) or flat SLB ($r_2 = \infty$) containing anionic lipids. In this case, the contact occurs primarily via the formation of bonds between ionizable and anionic lipids. These bonds can be viewed as relatively short flexible tethers of length l which is much shorter than the LNP radius. In this approximation, the radius of the contact region is given by (the derivation is similar to that for Eq. (7) in [36])

$$\rho = \left(\frac{2 l r_1 r_2}{r_1 + r_2}\right)^{1/2}. \tag{22}$$

The area of this region and the number of lipids on its lower or upper sides can accordingly be represented as

$$\sigma = \pi \rho^2 = \frac{2\pi l r_1 r_2}{r_1 + r_2}, \tag{23}$$

$$n = \frac{\sigma}{s} = \frac{2\pi l r_1 r_2}{s(r_1 + r_2)}. \tag{24}$$

The statistics of lipids in the contact region can be described by approximating this region by two adjacent fragments of 2D lattices. In particular, a pair of adjacent lattice sites (one belongs to the upper fragment and another one belongs to the lower fragment) can be in five states including (i) both sites in the background state, (ii) one site with a neutral ionizable lipid and another site in the background state, (iii) one site with a neutral ionizable lipid and another site with an anionic lipid, (iv) one site state with an ionized ionizable lipid and another site in the background state, and (v) one site state with an ionized ionizable lipid and another site with an anionic lipid. States (i) and (ii) are neutral because the sites do not contain charges. State (v) is neutral as well because the charges of the charges of ionizable and anionic lipids balance each other. For global neutrality, the charge of an ionizable or anionic lipid in states (iii) and (iv) should be balanced by the charge in solution. This is, however, energetically costly because the contact region is thin ($l \sim 0.5$ nm). For this reason, the latter states can be neglected. With this simplification, the two-site grand canonical function can be represented as as a sum of three terms corresponding to states (i), (ii), and (v),

$$S_{\rm cont} = 1 + \exp\left(\frac{\mu_{\rm il}}{k_{\rm B}T}\right) + \exp\left(\frac{\mu_{\rm al} + \mu_{\rm il} + \mu_{\rm H^+} - E_{\rm cont}}{k_{\rm B}T}\right), \tag{25}$$

where $E_{\rm cont} < 0$ is the pair interaction between ionizable and anionic lipids. The probabilities of states (i), (ii), and (v) can be obtained by dividing the corresponding terms in $S_{\rm cont}$ by $S_{\rm cont}$.

In the context under consideration, we need (see below) the probability that there is no pair interaction between ionizable and anionic lipids, i.e., that a pair of sites is in states (i) or (ii). This probability is given by

$$P_0 = \left[1 + \exp\left(\frac{\mu_{\rm il}}{k_{\rm B}T}\right)\right] \Big/ S_{\rm cont}. \tag{26}$$

Using Eqs. (25) and (26), one should take into account that the fractions of ionizable and anionic lipids in the contact area can be larger than those outside this area. This redistribution of lipids, however, can hardly change the fractions of ionizable and anionic lipids outside the area because the area of the contact region [Eq. (23)] is much smaller than the LNP external area. Practically, this means that the chemical potentials in Eqs. (25) and (26) describing the contact region are determined by Eqs. (17) and (21) obtained for lipids outside the contact region. In other words, the chemical potentials in Eqs. (25) and (26) for the contact region can be considered as external parameters (with respect to this region).

In the case of oppositely charged LNPs or a LNP and SLB, Eqs. (25) and (26) can be employed to describe the LNP detachment events. In particular, we can consider that the detachment rate constant is approximately proportional to a product of the probabilities of rupture of all the bonds, i.e.,

$$k_{\rm d} \propto P_0^n. \tag{27}$$

In fact, P_0^n determines the Arrhenius dependence of $k_{\rm d}$ [as in Eq. (13)], and accordingly the detachment activation energy can be represented as

$$E_{\rm a} \simeq -nk_{\rm B}T \ln(P_0). \tag{28}$$

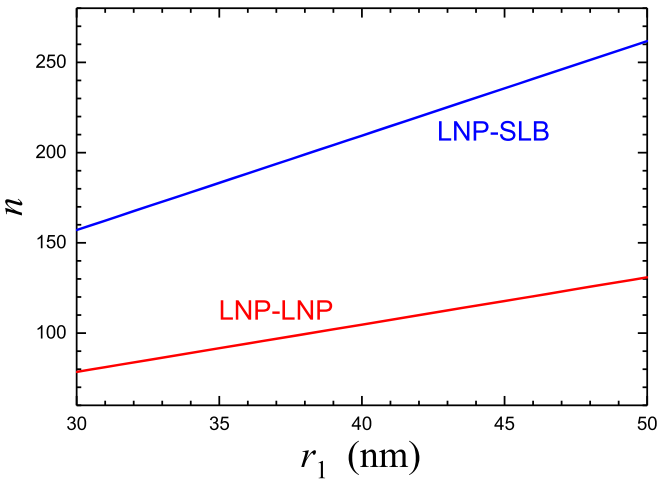

FIG. 4. Number of lipids on the lower or upper sides of the contact between (i) LNPs of the same size and (ii) a LNP and SLB as a function of the LNP radius according to Eq. (24) with $l = 0.5$ nm.

Taking into account that n is proportional to $r_1 r_2/(r_1 + r_2)$ [Eq. (24)], $E_{\rm a}$ is proportional to $r_1 r_2/(r_1 + r_2)$ as well and can be described by Eq. (14). The applicability of Eq. (14) in both cases is just a consequence of the fact that the contact area is proportional to $r_1 r_2/(r_1 + r_2)$ [Eq. (23)].

If the H^+ concentration is low (pH is large), the H^+ chemical potential is large and negative, and accordingly the third term in Eq. (25) is negligible compared to the first and second terms. In this limit, P_0 determined by Eq. (26) is close to unity, the detachment activation energy [Eq. (28)] is low, and the detachment rate constant [Eq. (27)] is high. With increasing H^+ concentration (decreasing pH), the role of the third term in Eq. (25) increases, P_0 becomes smaller, the detachment rate constant becomes smaller as well, whereas the detachment activation energy becomes larger. These activation energy and rate constant depend on n linearly and exponentially, respectively. Typically, n is rather large (Fig. 4), and accordingly the dependence of $k_{\rm d}$ on the other parameters is extremely strong (Fig. 5). At the attachment-detachment equilibrium, this practically means that the population of LNP dimers or aggregates in solution (in the case of oppositely charged LNPs) or adsorbed LNP (in the LNP-SLB case) is nearly negligible due to rapid detachment as long as pH is sufficiently large. Then, with increasing pH, the LNP attachment becomes nearly irreversible, and this transition takes place in a very narrow range of pH. This super selectivity is a general feature of kinetic processes occurring with participation of reactants with multivalent interaction [37–40].

IV. DENATURATION OF LNPs AT SLB

The interaction of LNPs containing ionizable (cationic) lipids with an SLB containing anionic lipids is of interest in the context of academic studies. The formation of bonds between cationic and anionic lipids is energetically favorable, attachment of such LNPs to SLB is favourable as well, and, accordingly, under such conditions LNPs are expected to be unstable, i.e., can be denaturated or disintegrated (these terms can be used interchangeably). Although the available

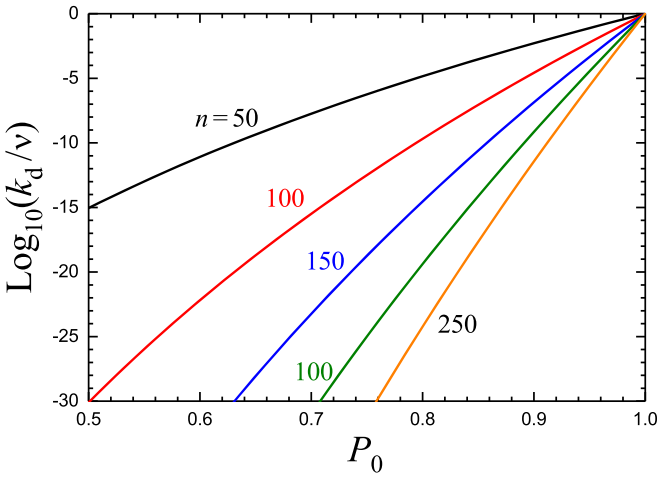

FIG. 5. Arrhenius factor of the detachment rate constant or, more specifically, k_d/ν as a function of the probability that there is no interaction in a pair of lipids in the contact region, according to Eq. (27). The number of lipids on the lower or upper sides of the contact region is indicated near the curves presented.

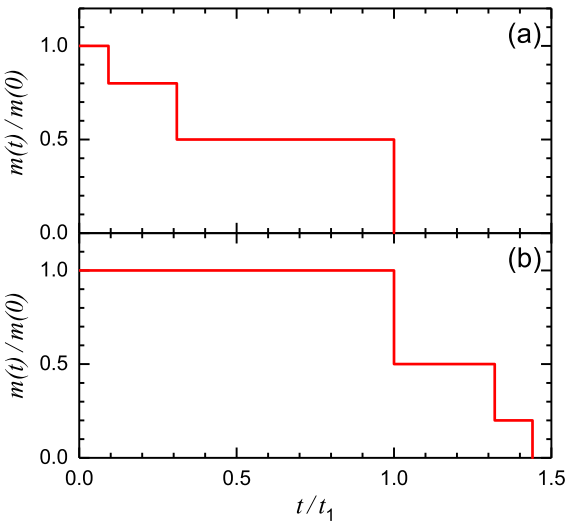

FIG. 6. Typical Monte Carlo kinetics of LNP denaturation after attachment to SLB calculated in the framework of the simplest three-state model with $\Delta m_1 = 0.5 m_{\mathrm{LNP}}$, $\Delta m_2 = 0.3 m_{\mathrm{LNP}}$, $\Delta m_3 = 0.2 m_{\mathrm{LNP}}$, $r_2 = 3 r_1$, and $r_2 = 10 r_1$. The LNP mass is shown as a function of time which is normalized to the time, t_1, corresponding to the maximum stepwise transfer of the LNP mass, $\Delta m_1 = 0.5 m_{\mathrm{LNP}}$, to SLB (for arrays of such kinetics, one has $\langle t_1 \rangle = 1/r_1$). The whole process occurs (a) in parallel or (b) sequentially. To naturally show the kinetics, the difference between rate constants r_1, r_2, and r_3 is chosen to be not too large. In reality, it can be much larger, and accordingly in experiments some of the stepwise transitions can be smeared and/or not registered.

conceptual mechanisms of the endosomal escape (Refs. [7,8]; reviewed in the Inroduction) imply LNP denaturation (or disintegration), the specifics of this process are now open for debate. In general, the denaturation of such mesoscopic particles as LNPs may occur via two alternative scenarios depending on the amount of matter transferred during elementary events. One gradual scenario implies numerous acts of transfer of small amount of matter. A typical example is disappearance of small nanoparticles during Ostwald ripening via evaporation and attachment of single atoms. Another stepwise scenario includes one or a few activated events of reconfiguration and denaturation of large counterparts of a nanoparicle. The latter scenario is possible and likely provided a nanoparticle is heterogeneous on the relatively large length scale which is only three or four times smaller than the nanoparticle size. As already mentioned in Sec. II A, the likely LNP structures are of this category, and accordingly their denaturation is expected to occur via the second scenario, i.e., via stepwise reconfiguration and denaturation of their large counterparts. Physically, each such "stepwise" subprocess is expected to include slow nucleation including transfer of small amount of lipids from a LNP to SLB and then rapid transfer of the main part of lipids forming a part of a LNP.

Accurate full-scale simulation of the above-described stepwise subprocesses is hardly possible at present. Phenomenologically, one can distinguish here two alternatives, with denaturation steps occurring in parallel or sequentially. At the simplest level, both alternatives can be mimicked by representing the whole process as a set of substeps of local redistribution of lipid mass, Δm_i, from a LNP to SLB with rate constants r_i. Substeps with larger Δm_i are expected to occur with smaller r_i. In the case of substeps running in parallel, this means that rapid substeps with smaller Δm_i are expected to be followed by slower substeps with larger Δm_i. In the case of substeps running sequentially, rapid substeps with smaller Δm_i may occur after slower substeps with larger Δm_i. The simplest three-state kinetics of these categories are shown in Fig. 6. More specific results illustrating the kinetics under consideration can be obtained by using the Monte Carlo lattice models or coarse-grained molecular dynamics (the latter method is briefly reviewed in, e.g., [41]).

V. CONCLUSION

The key ingredients of and conclusions drawn from the analysis presented above are as follows.

(i) I have described how the extent of protonation of ionizable lipids located at the surface of LNPs depends on the H^+ concentration by using the phenomenological Langmuir-Stern and Poisson-Boltzmann models with continuum distribution of charges and the dipole model with discrete charges. In both approaches, with physiologically oriented parameters, the H^+ adsorption isotherms are predicted to be close to Langmuirian provided the fraction of ionizable lipids is smaller than 0.5. If this fraction is larger, the isotherms become broader, but not dramatically. These predictions are instructive because *a priori* one could expect that the nonideality of the isotherms becomes well visible at smaller fractions of ionizable lipids. In particular, the results obtained allow one to understand why the generic experiments (Fig. 2 in Ref. [42]) performed with 70–90-nm-sized LNPs containing 40 mole % of ionizable lipids of four types indicate that the H^+ adsorption isotherms are close to Langmuirian in all four cases.

(ii) I have scrutinized the the interaction between charged ∼100-nm-sized LNPs and their interaction with SLB by using the DLVO-type theory and lattice-gas model. In this case, the

attractive van der Waals interaction is relatively weak, the hydration interaction is repulsive, and these interactions alone do not result in long-term association of LNPs or attachment of LNPs to SLB. If the charges of LNPs and SLB are of the same sign, the long-term association or attachment is not likely either, and this is in agreement with the fact that there are no experimental reports about observation of these phenomena. If the charges are opposite, the association or attachment is possible. It has been described at the DLVO and lattice-gas levels. In particular, the results obtained allow one to estimate the size of the contact region (provided a LNP is not deformed) and the number of lipid-lipid bonds in this region. This can be useful for interpretation of experiments with LNPs at cell-membrane mimics.

(iii) I have briefly discussed denaturation of a LNP during its interaction with an SLB and argued that it is expected to occur via a few stepwise transitions. This conclusion is of interest in the context of interpretation of experiments with LNPs at cell-membrane mimics. Conceptually, the stepwise scenario can be useful in the context of the LNP endosomal escape as well. In the available literature (see, e.g., reviews [7,8]), this scenario is not discussed.

All the subjects discussed and scrutinized above merit obviously additional attention.

ACKNOWLEDGMENT

The author thanks Prof. F. Höök for useful discussions.

[1] L. A. Lane, Physics in nanomedicine: Phenomena governing the *in vivo* performance of nanoparticles, Appl. Phys. Rev. **7**, 011316 (2020).

[2] J. A. Jackman *et al.*, Biomimetic nanomaterial strategies for virus targeting: Antiviral therapies and vaccines, Adv. Funct. Mater. **31**, 2008352 (2021).

[3] M. J. Mitchell, M. M. Billingsley, R. M. Haley, M. E. Wechsler, N. A. Peppas, and R. Langer, Engineering precision nanoparticles for drug delivery, Nat. Rev. Drug. Discov. **20**, 101 (2021).

[4] X. Hou, T. Zaks, R. Langer, and Y. Dong, Lipid nanoparticles for mRNA delivery, Nat. Rev. Mater. **6**, 1078 (2021).

[5] M. P. Stewart, A. Lorenz, J. Dahlman, and G. Sahay, Challenges in carrier-mediated intracellular delivery: moving beyond endosomal barriers, WIREs Nanomed. Nanobiotechn. **8**, 465 (2016).

[6] P. S. Kowalski, A. Rudra, L. Miao, and D. G. Anderson, Delivering the messenger: advances in technologies for therapeutic mRNA delivery, Mol. Ther. **27**, 710 (2019).

[7] S. A. Smith, L. I. Selby, A. P. R. Johnston, and G. K. Such, The endosomal escape of nanoparticles: toward more efficient cellular delivery, Bioconjugate Chem. **30**, 263 (2019).

[8] I. M. S. Degors, C. Wang, Z. U. Rehman, and I. S. Zuhorn, Carriers break barriers in drug delivery: endocytosis and endosomal escape of gene delivery vectors, Acc. Chem. Res. **52**, 1750 (2019).

[9] S. Das, M. Vera, V. Gandin, R. H. Singer, and E. Tutucci, Intracellular mRNA transport and localized translation, Nat. Rev. Mol. Cell Biol. **22**, 483 (2021).

[10] M. Mendozza, L. Caselli, A. Salvatore, C. Montis, and D. Berti, Nanoparticles and organized lipid assemblies: from interaction to design of hybrid soft devices, Soft Matter **15**, 8951 (2019).

[11] J. Park and W. Lu, Interaction of nanoparticles with lipid layers, Phys. Rev. E **80**, 021607 (2009).

[12] X. Yi, X. Shi, and H. Gao, Cellular Uptake of Elastic Nanoparticles, Phys. Rev. Lett. **107**, 098101 (2011).

[13] N. Shimokawa, H. Ito, and Y. Higuchi, Coarse-grained molecular dynamics simulation for uptake of nanoparticles into a charged lipid vesicle dominated by electrostatic interactions, Phys. Rev. E **100**, 012407 (2019).

[14] Y. Zhang, L. Li, and J. Wang, Tuning cellular uptake of nanoparticles via ligand density: Contribution of configurational entropy, Phys. Rev. E **104**, 054405 (2021).

[15] V. P. Zhdanov, Multivalent ligand-receptor-mediated interaction of small filled vesicles with a cellular membrane, Phys. Rev. E **96**, 012408 (2017).

[16] V. P. Zhdanov, Kinetics of lipid-nanoparticle-mediated intracellular mRNA delivery and function, Phys. Rev. E **96**, 042406 (2017).

[17] V. P. Zhdanov, mRNA function after intracellular delivery and release, Biosystems **165**, 52 (2018).

[18] V. P. Zhdanov, Intracellular miRNA or siRNA delivery and function, Biosystems **171**, 20 (2018).

[19] V. P. Zhdanov, Intracellular RNA delivery by lipid nanoparticles: Diffusion, degradation, and release, Biosystems **185**, 104032 (2019).

[20] V. P. Zhdanov, How nanoparticles can induce dimerization and aggregation of cells in blood, Biosystems **210**, 104551 (2021).

[21] V. P. Zhdanov, Kinetic aspects of virus targeting by nanoparticles in vivo, J. Biol. Phys. **47**, 95 (2021).

[22] M. A. Oberli, A. M. Reichmuth, J. R. Dorkin, M. J. Mitchell, O. S. Fenton, A. Jaklenec, D. G. Anderson, R. Langer, and D. Blankschtein, Lipid nanoparticle assisted mRNA delivery for potent cancer immunotherapy, Nano Lett. **17**, 1326 (2017).

[23] S. S. W. Leung and C. Leal, The stabilization of primitive bicontinuous cubic phases with tunable swelling over a wide composition range, Soft Matter **15**, 1269 (2019).

[24] M. Y. Arteta *et al.*, Successful reprogramming of cellular protein production through mRNA delivered by functionalized lipid nanoparticles, Proc. Natl. Acad. Sci. USA **115**, E3351 (2018).

[25] L. Koopal, W. Tan, and M. Avena, Equilibrium mono- and multicomponent adsorption models: from homogeneous ideal to heterogeneous non-ideal binding, Adv. Colloid Interface Sci. **280**, 102138 (2020).

[26] A. J. Bard and L. R. Faulkner, *Electrochemical Methods: Fundamentals and Applications* (Wiley, New York, 2001).

[27] A.A. Kornyshev, Double-layer in ionic liquids: paradigm change?, J. Phys. Chem. B **111**, 5545 (2007).

[28] A. Härtel, Structure of electric double layers in capacitive systems and to what extent (classical) density functional

theory describes it, J. Phys.: Condens. Matter **29**, 423002 (2017).

[29] Y. Zhang and J. Huang, Treatment of ion-size asymmetry in lattice-gas models for electrical double layer, J. Phys. Chem. C **122**, 28652 (2018).

[30] G. V. Bossa and S. May, Debye-Hückel free energy of an electric double layer with discrete charges located at a dielectric interface, Membranes **11**, 129 (2021).

[31] V. P. Zhdanov, Thermal desorption and surface diffusion complicated by dipole-dipole interaction between adsorbed particles, Surf. Rev. Lett. **05**, 977 (1998).

[32] V. P. Zhdanov (unpublished).

[33] H. Ohshima, Fundamentals, in *Electrical Phenomena at Interfaces and Biointerfaces: Fundamentals and Applications in Nano-, Bio-, and Environmental Sciences*, edited by H. Ohshima (Wiley, Hoboken, 2012), Part I, Secs. 1–4.

[34] V. P. Zhdanov, Nanoparticles without and with protein corona: van der Waals and hydration interaction, J. Biol. Phys. **45**, 307 (2019).

[35] J. Y. Walz and E. Ruckenstein, Comparison of the van der Waals and undulation interactions between uncharged lipid bilayers, J. Phys. Chem. B **103**, 7461 (1999).

[36] V. P. Zhdanov, Diffusion-limited attachment of nanoparticles to flexible membrane-immobilized receptors, Chem. Phys. Lett. **649**, 60 (2016).

[37] T. Curk, J. Dobnikar, and D. Frenkel, Optimal multivalent targeting of membranes with many distinct receptors, Proc. Natl. Acad. Sci. USA **114**, 7210 (2017).

[38] M. Liu *et al.*, Combinatorial entropy behaviour leads to range selective binding in ligand-receptor interactions, Nat. Commun. **11**, 4836 (2020).

[39] V. P. Zhdanov, Kinetics of virus entry by endocytosis, Phys. Rev. E **91**, 042715 (2015).

[40] T. Curk, J. Dobnikar, and D. Frenkel, Design principles for super selectivity using multivalent interactions, in *Multivalency: Concepts, Research and Applications*, edited by J. Huskens, L. Prins, R. Haag, and B. J. Ravoo (Wiley, Oxford, 2018), Chap. 3, pp. 75–102.

[41] S. Y. Joshi and S. A. Deshmukh, A review of advancements in coarse-grained molecular dynamics simulations, Mol. Simul. **47**, 786 (2021).

[42] M. Jayaraman *et al.*, Maximizing the potency of siRNA lipid nanoparticles for hepatic gene silencing in vivo, Angew. Chem., Int. Ed. **51**, 8529 (2012).